



Neutron scattering/Diffusion de neutrons

# Monitoring molecular motion in nano-porous solids

Stéphane Rols<sup>a,b,\*</sup>, Hervé Jobic<sup>c</sup>, Helmut Schober<sup>a</sup>

<sup>a</sup> Institut Laue-Langevin, 6, rue Jules-Horowitz, BP 156, 38042 Grenoble cedex 9, France

<sup>b</sup> Laboratoire des colloïdes, verres et nanomatériaux, Université de Montpellier, 34095 Montpellier cedex 5, France

<sup>c</sup> Institut de recherches sur la catalyse et l'environnement, 2, avenue A. Einstein, 69626 Villeurbanne, France

Available online 24 October 2007

## Abstract

In this article, the important role of neutron spectroscopy techniques for the study of the dynamics of molecules hosted inside cavities at the nanometer scale is described. Three different complex systems are highlighted: alkanes with variable length inside zeolitic matrices, C<sub>60</sub> fullerene chains inside single wall carbon nanotubes, and inert gas (N<sub>2</sub>, Xe) molecules inside water clathrates.

**To cite this article:** S. Rols et al., C. R. Physique 8 (2007).

© 2007 Académie des sciences. Published by Elsevier Masson SAS. All rights reserved.

## Résumé

**Suivre les mouvements moléculaires dans les solides nano-poreux.** Cet article illustre le rôle majeur de la spectroscopie neutronique dans l'étude de la dynamique des molécules insérées dans des cavités de taille nanométrique, à travers l'étude de trois systèmes complexes : des alcanes de taille variable confinés à l'intérieur de matrices zéolitiques, des chaînes unidimensionnelles de C<sub>60</sub> dans des nanotubes monofeuillets de carbone et des gaz inertes (N<sub>2</sub>, Xe) dans les clathrates d'eau. **Pour citer cet article :** S. Rols et al., C. R. Physique 8 (2007).

© 2007 Académie des sciences. Published by Elsevier Masson SAS. All rights reserved.

**Keywords:** Neutron scattering; Neutron spectroscopy; Zeolites; Nanotubes; Fullerenes; Clathrates; Diffusion; Vibrations; Confinement

**Mots-clés :** Diffusion neutronique ; Spectroscopie neutronique ; Zeolites ; Nanotubes ; Fullerènes ; Clathrates ; Diffusion ; Vibrations ; Confinement

## 1. Introduction

The scientific field concerned with nano-porous media is continuously expanding. In addition to naturally occurring materials there is a growing number of engineered cage and channel structures. Nano-pores are ideally suited to host guest atoms or molecules, which have the potential of strongly modifying the physical and chemical properties of the material. In the extreme case the guest molecules are indispensable for the stability of the cage itself. A typical example for this strong guest–host symbiosis is clathrate hydrates. The simple fact that we talk about guest–host systems already indicates that we are dealing with clearly identifiable subsystems. Two questions are of particular interest in this context: How do the properties of the host matrix react to the doping with guest molecules, and how does the geometrical confinement alter the properties of the guest? In particular the latter question has received much

\* Corresponding author.

E-mail address: [rols@ill.fr](mailto:rols@ill.fr) (S. Rols).

attention during the last years. Phase and/or glass transition, transport properties, local structure, mobility etc. are predicted to be different from the bulk when the material is confined in a domain of nanometer size.

The interaction between the porous matrix and the guest molecules, as well as the relative size of the guest and of the pore, are the key factors that determine the guest–host system. Recent development of new host matrices with pores of controlled shape and dimension on the nanometer scale strongly enhance the experimental possibilities by allowing the tailoring of the samples to the scientific question. As we will show, inelastic neutron scattering stands out as a very valuable technique to gain insight into the guest–host interaction as well as the dynamics related properties of these complex systems.

In this paper, we review some recent advances into the understanding of the dynamical properties of molecules hosted inside cavities of nanometer scale taking advantage of the use of inelastic and quasielastic neutron scattering. The different porous matrices are zeolites, carbon nanotubes and clathrates, containing alkanes of different length, C<sub>60</sub> molecules and inert gas, respectively. In the case of zeolites we concentrate on the technologically important translational transport properties of molecular chains in a three-dimensional cage network. Nanotubes filled with C<sub>60</sub> are an example of a rigid spherical object trapped within a rigid tube. Rotational dynamics becomes important in that case. Clathrate hydrates finally deal with molecules in cages not connected to each other. Translational diffusion is not possible in that case and the dynamics is described in terms of a tumbling (small molecules weakly bound in a large cage) or vibrational motion (molecule fills cage or molecule is strongly bound).

## 2. Zeolites

Several neutron techniques are being used to study zeolitic systems. The structure and the localisation of ions and molecules have been determined by powder neutron diffraction. Some works by small-angle neutron scattering (SANS) concern the mechanism of formation of zeolite crystals and the clustering of adsorbed molecules. The vibrational modes of zeolite frameworks and of molecules have been measured by inelastic neutron scattering (INS). Finally, the rotational and translational motions of adsorbed molecules have been characterized by quasi-elastic neutron scattering (QENS).

The diffusion of molecules in porous media can be studied by a large variety of methods. This explains the large number of definitions of diffusion coefficients (or diffusivities) which can be found in the literature [1]. Pulsed-field gradient (PFG) NMR and incoherent QENS measure the self-diffusivity,  $D_s$ , at thermodynamic equilibrium. Since hydrogen has the largest neutron incoherent cross-section, the first neutron measurements concerning diffusion in zeolites dealt with hydrogenated molecules.

In separation or catalytic applications, it is the transport diffusivity,  $D_t$ , which matters (this quantity is also named Fickian or chemical diffusivity). Transport diffusivities are traditionally measured under non-equilibrium conditions. Fick's first law defines  $D_t$  as the proportionality factor between the flux  $J$  and a concentration gradient:

$$J = -D_t \nabla c \quad (1)$$

Despite extensive work in the last decade, large discrepancies still persist between the various experimental techniques which measure diffusion in zeolites. One of the difficulties is to compare self- with transport diffusivities. One expects that  $D_s$  and  $D_t$  will have a different concentration dependence. Comparisons between PFG NMR, QENS, and molecular dynamics (MD) simulations could only be made in the past at the level of  $D_s$ . At equilibrium, one can now obtain experimentally  $D_t$  using coherent neutron scattering [2]. From equilibrium MD simulations, one cannot derive  $D_t$ , but one can determine the corrected diffusivity,  $D_o$ , from the fluctuations in an equilibrium density distribution. This was accomplished for Ar in AlPO<sub>4</sub>-5 using the Green–Kubo formalism [3]. Moreover, the calculations being performed in reciprocal space, the variation of the diffusivity upon the wave vector can be used to check when the system is in the linear regime [3].

The transport and corrected diffusivities are linked by considering that the driving force for diffusion is the chemical potential gradient, and not the concentration gradient; one obtains:

$$D_t(c) = D_o(c) \left( \frac{d \ln p}{d \ln c} \right) = D_o(c) \Gamma \quad (2)$$

where  $p$  is the partial pressure of the adsorbed gas and  $\Gamma$  is the thermodynamic correction factor. One approximation which can be found in the literature is to replace  $D_o$  by  $D_s$ . However, the self, transport, and corrected diffusivities

are only equal in the limit of zero concentration. All these diffusivities can have a different concentration dependence, and this is indeed what has been evidenced recently, both by experiments and by simulations.

### 2.1. Linear alkanes in silicalite

Silicalite is a recent crystalline form of silica. The structure of silicalite consists of straight channels interconnected by sinusoidal channels, both having a free diameter of about 5.5 Å. When some Si atoms are substituted by Al atoms, protons or cations compensate the negative charges of the  $\text{AlO}_4^-$  tetrahedra. Both ZSM-5 and silicalite (structure code MFI) have found wide applications in catalysis or in the separation of gases and liquids. Zeolitic membranes, i.e. membranes where the zeolite is either deposited on or synthesised inside a ceramic support, are often based on the MFI structure.

The diffusion of alkanes in MFI-type zeolites is probably the system which has been the most studied by various experimental and theoretical methods. The magnitude of the diffusion coefficients in silicalite has been a point of controversy for about 20 years. The ‘macroscopic’ measurements yield values which are orders of magnitude lower than those obtained by the ‘microscopic’ techniques: PFG NMR and QENS [1]. In the 1990s, a hierarchical simulation technique based on coarse-grained Brownian dynamics and transition-state theory was performed on *n*-alkanes ranging from  $\text{C}_1$  (methane) to  $\text{C}_{20}$  in silicalite [4]. No experimental data existed at that time for *n*-alkanes longer than  $\text{C}_6$ . QENS measurements were performed later for chains up to  $\text{C}_{14}$ , but in ZSM-5 zeolite [5].

The diffusion of *n*-alkanes in MFI samples was recently revisited by QENS and PFG NMR [6,7]. The self-diffusivities are shown in Fig. 1 as a function of chain length.

The new QENS results are in much better agreement with the theoretical predictions. For  $\text{C}_{10}$ , the difference is less than a factor of 2, which is negligible considering the experimental error on the QENS values and the error associated with the coarse-graining procedure in the simulations. Those theoretical values are higher than QENS results as expected from simulations made in a perfect crystalline structure and for an infinitely diluted sorbed phase. QENS measurements are performed on real crystals at a finite loading, corresponding to 12 carbon atoms per unit cell, and it is well known that the self-diffusivity decreases with increasing loading.

Both techniques establish that the low-occupancy self-diffusivity is a monotonic function which decreases less than linearly with chain length. QENS/simulation self-diffusivities are systematically higher than PFG-NMR

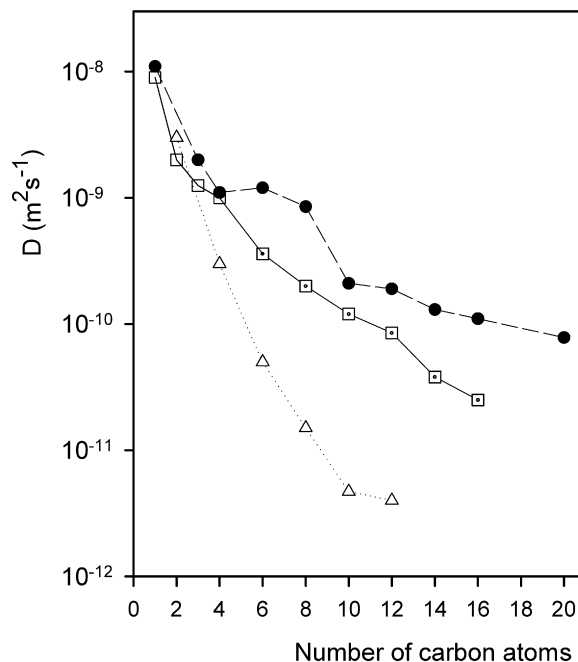


Fig. 1. Self-diffusion coefficients, obtained at 300 K by different techniques, for *n*-alkanes in silicalite: (●) hierarchical simulations [4], (□) QENS in ZSM-5 [5], (□) QENS in silicalite [7], (△) PFG NMR [6]. (Adapted from Ref. [7].)

diffusivities [7], indicating that the PFG-NMR method, with its larger length scale of observation ( $\mu\text{m}$ ), is more sensitive than QENS/simulation to defects in the crystal structure. The presence of intracrystalline barriers (defects, twinning, etc.) is now recognised as the most probable explanation for the discrepancies which have been reported in the literature for the past 30 years.

The activation energy for self-diffusion at low occupancy is around 5 kJ/mol for normal alkanes up to  $\text{C}_6$  but rises with chain length beyond  $\text{C}_8$  to approximately 15 kJ/mol for  $\text{C}_{16}$ . Molecular simulations relate this to the fact that alkanes longer than  $\text{C}_6$  cannot fit entirely within channel segments and have to protrude into or straddle channel intersections, their translational motion requiring some degree of conformational isomerization [7].

## 2.2. Linear alkanes in LTA zeolite, the ‘window effect’

LTA zeolite is part of numerous adsorption processes in the field of refining petrochemicals or natural gas treatment. The structure consists of a cubic array of cages (diameter  $\approx 11 \text{ \AA}$ ), interconnected by windows. In the calcium form, the effective diameter of the windows is close to  $5 \text{ \AA}$ , hence the product name: 5A. One of the most extensively used properties of 5A zeolite is the ability to adsorb linear alkanes while rejecting branched ones. This property is devoted to the production of highly branched  $\text{C}_5$ – $\text{C}_6$  paraffins for octane upgrading in gasoline or for supplying linear  $\text{C}_{10}$ – $\text{C}_{14}$  alkanes for linear alkylbenzene synthesis.

The diffusion of *n*-alkanes in 5A zeolite is too slow to be measured on time-of-flight or back-scattering instruments, but it is accessible by the neutron spin-echo technique. Since coherent scatterers yield a better signal in NSE, deuterated *n*-alkanes were used for the measurements [8]. Normalised intermediate scattering functions measured at the same experimental conditions for three *n*-alkanes in 5A zeolite, at 475 K, are shown in Fig. 2. Since a faster decay corresponds to a larger diffusion coefficient, a mere look at Fig. 2 leads to the conclusion that the diffusivity increases with increasing chain length, in the sequence  $\text{C}_8 < \text{C}_{10} < \text{C}_{12}$ . This is completely counter-intuitive. From the data obtained at two different  $Q$  values and using a jump diffusion model, the diffusion coefficients shown in Fig. 3 could be derived. One finds that the transport diffusivity has a minimum at  $\text{C}_8$  and a maximum at  $\text{C}_{12}$ . Since the loading was selected such that the number of carbon atoms per cavity stays constant (i.e. 12 C per  $\alpha$ -cage), a similar maximum is expected for the corrected diffusivity, after correcting for the thermodynamic factor. The activation energy is larger for  $\text{C}_8$ ,  $41 \text{ kJ mol}^{-1}$ , than for  $\text{C}_{12}$ ,  $35 \text{ kJ mol}^{-1}$ .

The maximum of diffusivity, as well as the minimum in the activation energy, observed for  $\text{C}_{12}$  in 5A zeolite can be explained by the ‘window effect’. This term was coined by Goring to interpret anomalous transport results obtained in zeolite T, where he found that molecules in the  $\text{C}_{12}$  range diffused about 2 orders of magnitude faster than those in the  $\text{C}_8$  range [9]. This concept was developed to designate the higher transmittance of the erionite cages for molecules of a given critical length. However, the experimental conditions used by Goring have been criticized, and since no

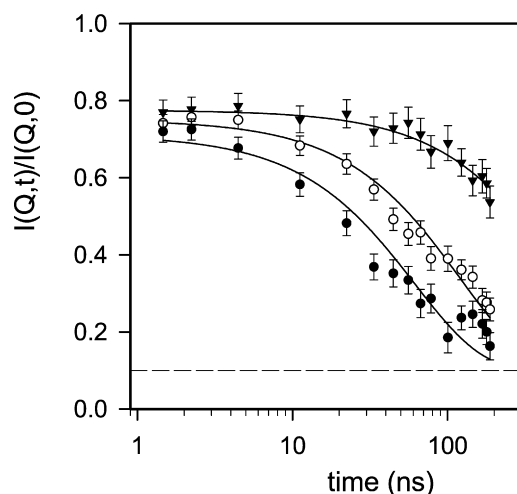


Fig. 2. Normalised intermediate scattering functions obtained for some *n*-alkanes in 5A zeolite, at 475 K: ( $\blacktriangledown$ )  $\text{C}_8$ , ( $\circ$ )  $\text{C}_{10}$ , and ( $\bullet$ )  $\text{C}_{12}$ , ( $Q = 0.2 \text{ \AA}^{-1}$ ).

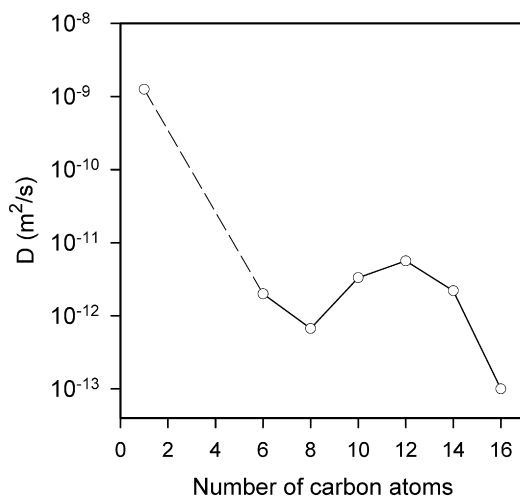


Fig. 3. Transport diffusivities obtained by NSE at 475 K for linear alkanes in 5A zeolite, as a function of the carbon number.

other group could reproduce his periodic variation in diffusivity, the existence of this window effect is still disputed, although some recent molecular simulations predict its occurrence in various zeolite structures. The interpretation is the following: a  $C_8$  molecule fits well into a cavity, whereas  $C_{12}$  is too long to sit comfortably in a cage and adopts a conformation where one end of the molecule extends through a window. The energy barrier (largely entropic) is thus easier to cross for the longer molecule, leading to a higher diffusivity and to lower activation energy. For molecules longer than  $C_{12}$ , an increasing steric hindrance will again lead to a decrease of the diffusivity.

### 3. Peapods

Single Wall carbon NanoTubes (SWNT) are long ‘all carbon’ molecules that can be viewed as graphene sheets rolled up into a cylindrical shape to form a tube [10]. They self organize onto a 2D hexagonal lattice which is often referred to as a bundle of SWNT. Their unique 1D character and C–C  $sp^2$  hybridization are responsible for their exceptional electronic, optical and mechanical properties which are the subject of an intense theoretical and experimental activity. Apart from their intrinsic interesting physical properties, SWNT have also been extensively used as molecular templates for adsorption of molecules and/or atoms. The goal is to use the different adsorption sites that a SWNT bundle offers, to study the influence of confinement on the physical properties of the adsorbed species or the influence of the guest molecules on the properties of the nanotubes (in an attempt to modify their electronic conductivity in the case of doping for example).

Neutron Diffraction and inelastic neutron scattering have been used to study the structure and the dynamics of raw SWNT samples [11]. Due to the very high scattering cross section of hydrogen and to the isotopic contrast technique intrinsic of neutron scattering, this experimental technique is particularly adapted to the study of the intercalated/adsorbed phases of SWNT in general and in hydrogen containing molecules in particular. As an example, the influence of the nanotube confinement on the physical properties of water has recently been studied by diffraction and inelastic neutron scattering. It has been shown that the water molecules are adsorbed inside the nanotubes and form a first layer made of water molecules organized on a square lattice encapsulating a 1D chain of water molecules [12]. This system is observed to have a much softer dynamics than any water phase known up to now.

In the present paper we are concerned with the study of the dynamics of the so-called peapods. They stand as 1D chains of  $C_{60}$  molecules adsorbed inside the hollow core of the SWNT. The study of the dynamics of the fullerenes confined inside the nanotubes has been limited to the measurement of a few Raman active modes that are intense enough to emerge from the high background due to the nanotube response. However, a careful study of the splitting of some  $A_g$  Raman active modes of a peapod sample suggested the  $C_{60}$  molecules have some mobility inside the nanotubes [13].

Inelastic neutron scattering has proved to be a powerful tool to give insight into the dynamics of the  $C_{60}$ . The density of vibrational states (VDOS) has been derived in the complete (0–200 meV) range allowing the development

and the verification of many numerical models. It was found that the  $C_{60}$  molecules form a plastic crystal (orientational disordered phase) at ambient temperature with the molecules rotating almost freely and independently one from the other [14,15]. This diffusive character gives rise to a large quasielastic signal. Due to the very isotropic geometry of the  $C_{60}$  combined to the isotropic geometry of the movement, the structure factor of the quasielastic signal has a very peculiar shape. In particular, it is very weak up to a value of  $2.5 \text{ \AA}^{-1}$ . This plastic phase experiences a first order phase transition at a temperature  $T_c \sim 255 \text{ K}$  [16] where the free rotations are blocked and replaced by librations featuring intense peaks located in the inelastic range around  $2.5 \text{ meV}$  [17].

Inelastic neutron scattering has also shown to be particularly efficient to characterize the nature of the interaction between adjacent  $C_{60}$  cages. Some charge transfer induced by doping the  $C_{60}$  phase and/or high pressure high temperature treatment has been found to create covalent bonds in between the  $C_{60}$  molecules. The large gap separating the intermolecular modes from the intramolecular vibrations of the  $C_{60}$  [8, 30 meV] is then progressively filled by the new modes involving the deformation of the intermolecular covalent bonds which is then found to be characteristic of the phase under study [18]. Such modes have been detected recently in as-prepared nanopeapods suggesting that a small fraction of the  $C_{60}$  present inside the nanotubes is polymerized [19]. Recent in-situ diffraction under high pressure and high temperature conditions has clearly shown the possibility to induce polymerization of the  $C_{60}$  inside the nanotubes [20]. The polymer phase is then found to be stable under normal  $P$  and  $T$  conditions. A simple heat treatment at a temperature of  $180^\circ\text{C}$  is then necessary to recover a monomer phase of the  $C_{60}$  [21].

We have used inelastic neutron scattering and coherent quasielastic neutron scattering to study the dynamics of the monomer phase of the  $C_{60}$  peapods. Prior to the experiment, the sample was baked at a temperature of  $300^\circ\text{C}$  under secondary vacuum in order to minimize the quantity of  $C_{60}$  in polymeric form inside the sample and to remove any trace of water/hydrogenous molecules that could be adsorbed inside the sample. Two sets of experiments were performed: one using the IN1BeF filter analyser spectrometer mounted on the hot source at the Institut Laue-Langevin. This spectrometer allows one to measure energy transfer ranging from  $30 \text{ meV}$  up to several hundreds of meV. The IN4C spectrometer is a time of flight spectrometer mounted on the thermal source at the ILL. A  $1.1 \text{ \AA}$  neutron incident wavelength was used which allowed the  $10$  to  $55 \text{ meV}$  energy range to be studied. The measurements were performed at  $10 \text{ K}$  on both instruments and for peapods and nanotubes samples. Moreover, measurements at  $150 \text{ K}$  and  $300 \text{ K}$  were also performed on the IN4C spectrometer. The signal was transformed into either the so-called generalized density of states (GDOS) or into the susceptibility depending on the most convenient representation (cf. Appendix A).

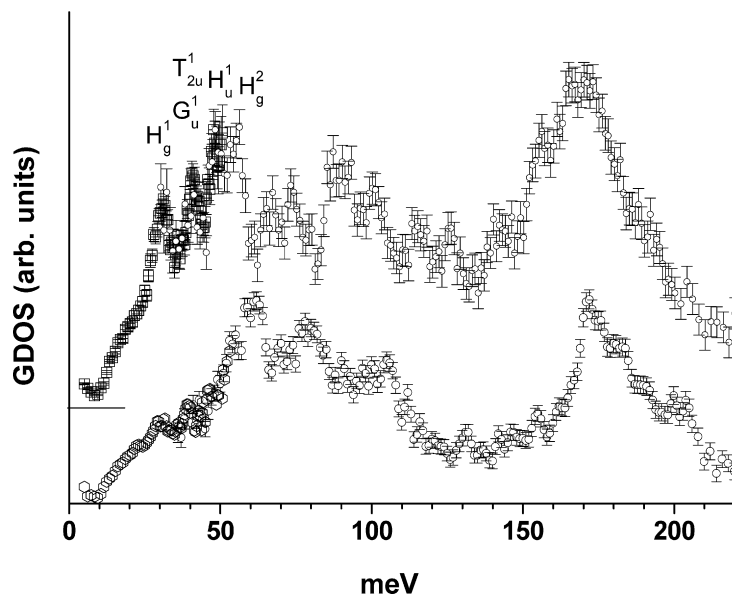


Fig. 4. The GDOS of a peapod sample (up: squares = IN4; circles = IN1BeF) and of a nanotubes sample (bottom: diamonds = IN4; circles = IN1BeF) in the complete energy range [10, 200 meV] ( $T = 10 \text{ K}$ ). The connection of the spectra obtained measuring the same sample on both spectrometers was done by scaling their intensity to make them match at  $40 \text{ meV}$ . Then the spectra have their intensity normalised to unity. An arbitrary shift of the peapods' GDOS was applied for clarity purpose.

Fig. 4 shows the GDOS of the peapods sample obtained using the combination of both instruments (upper curve) which is compared to the GDOS of the SWNT sample (lower curve). The GDOS of the peapods is observed to be very different from the one of the nanotube sample with additional features observed that can be attributed to the contribution of the intramolecular modes of the  $C_{60}$ . An isolated  $C_{60}$  molecule has 174 intramolecular vibrations. The highly symmetric icosahedron shape of the fullerene implies that a large number of the frequencies of these modes are degenerated which results in 46 distinct frequencies. The vibrations of a  $C_{60}$  molecule can be classified according to their symmetry [22]:

$$2A_g + A_u + 3T_{1g} + 4T_{1u} + 4T_{2g} + 5t_{2u} + 6G_g + 6G_u + 8H_g + 7H_u$$

When a  $C_{60}$  molecule is confined inside a nanotube and in the assumption of weak van der Waals interaction with it, its vibration frequencies are calculated to be weakly dispersive and almost not affected by the tube environment. In this case they give intense contributions to the total GDOS [23]. Therefore the contributions of the  $C_{60}$  intramolecular modes are superimposed to the GDOS of the nanotubes, which is clearly observed in the low-frequency part of the GDOS in Fig. 4. One can further assign each of the intense modes to the corresponding symmetry of the  $C_{60}$  vibration: as an example, the first intramolecular mode  $H_g^1$ —which is a 5 fold (H) mode, symmetric with regards to the inversion operation (g)—is observed at 33 meV.

Fig. 5 represents the susceptibility of the peapods measured at 10 K, 150 K and 300 K together with the corresponding GDOS. For excitations following a Bose dependence with temperature, their susceptibility should overlap (see next paragraph and [32]), which is not observed in this experiment. One generally attributes such a low-frequency signal and dependence to relaxation modes inducing the appearance of a quasielastic signal. This quasielastic contribution can be fitted by a Lorentzian function, the intensity and width of which is plotted on Fig. 6. At a temperature of 10 K, the broadening of the elastic line can no longer be measured. This indicates a lowering of the mobility of the  $C_{60}$  molecules. This sharpening is concomitant with the sharpening of the intramolecular modes, the width of which is strongly temperature sensitive (see Fig. 5 insert).

The peculiar dependence of the intensity of the quasielastic signal is characteristic of the  $C_{60}$  molecule and of an isotropic diffusion. One can reasonably attribute such diffusion to the rotations of the  $C_{60}$  inside the SWNT, the temperature of freezing of which is shifted to lower temperature ( $T_c < 150$  K) compared to the case of pure  $C_{60}$  ( $T_c \sim 255$  K). This is characteristic of the confinement of the molecule.

Inelastic neutron scattering and quasielastic neutron scattering are therefore observed to be very efficient tools to study the effect of confinement of the  $C_{60}$  inside the nano-pores formed by the interior of the nanotubes. It has been

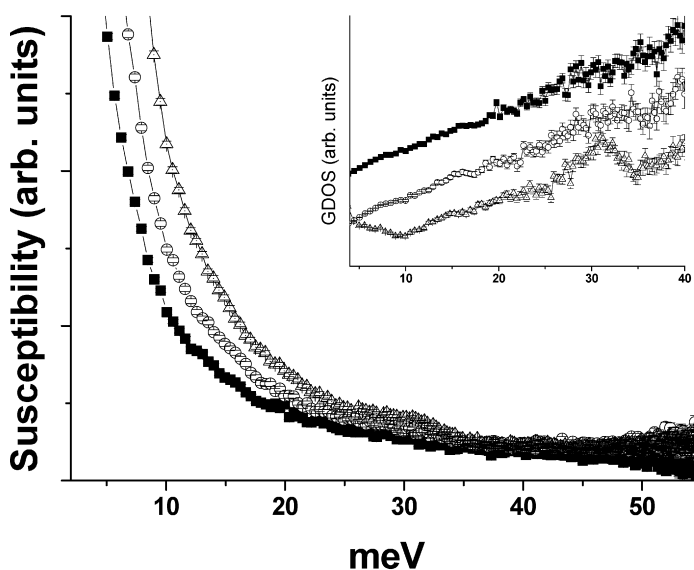


Fig. 5. Susceptibility of the peapods sample measured on the IN4 spectrometer using a  $1.1 \text{ \AA}$  incident wavelength at 10 K (triangle), 150 K (circles) and 300 K (squares). Insert: the corresponding generalized density of states emphasising the broadening of the  $H_g^1$  intramolecular mode of  $C_{60}$  at 33 meV upon heating.

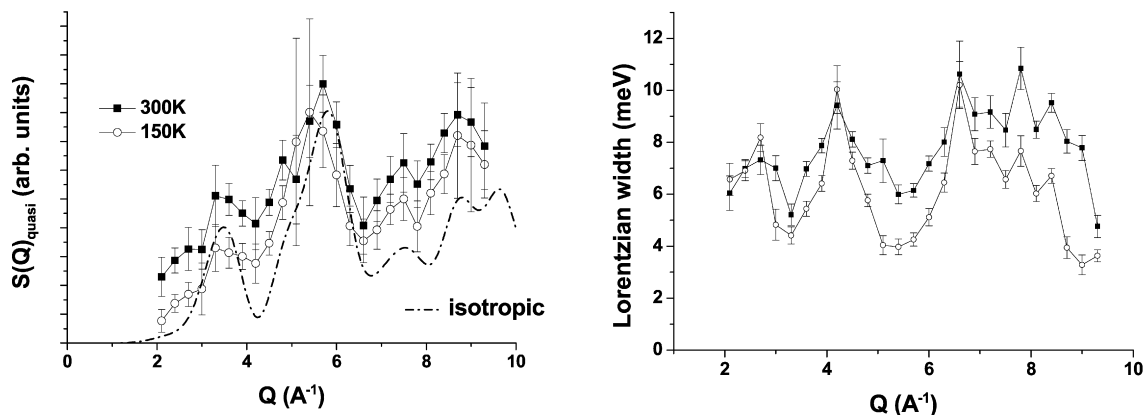


Fig. 6. Integrated intensity (left) and full width at half maximum (right) of a Lorentzian component fitted to the quasielastic signal of the peapod sample, as a function of the momentum transfer  $Q$  and at 300 K (squares) and 150 K (circles).

shown that the  $C_{60}$  intramolecular modes are not affected by the confinement as their frequencies are observed close to the position of those of the  $C_{60}$  in the gaseous state. The quasielastic signal observed in the temperature range from 150 K up to 300 K suggests a dynamical disorder of the  $C_{60}$  inside the nanotube. The freezing of the  $C_{60}$  diffusion that would lead to the appearance of inelastic features in the low frequency range has not been observed up to now. At 10 K, however, a sharpening of the inelastic features associated to the disappearance/sharpening of the quasielastic line suggest an important lowering of the  $C_{60}$  mobility. Further experiments are scheduled to follow the freezing of the  $C_{60}$  as a function of temperature. For this the low-frequency inelastic range will be studied in detail.

#### 4. Clathrates

Clathrate hydrates are open cage structures made-up of hydrogen-bonded water molecules (see Fig. 7). They are stabilized by the presence of guest molecules in the cages. Most low molecular weight gases (including  $O_2$ ,  $N_2$ ,  $CO$ ,  $CO_2$ ,  $CH_4$ , Ar, Kr and Xe) will form clathrate hydrates under certain pressure–temperature conditions. Clathrate hydrates were originally encountered as a nuisance during transport and storage of hydrocarbons. Since it became clear that methane hydrate, which is found in large quantities on the ocean sea floor and in permafrost regions, may constitute one of the major energy reserves of the planet this attitude has changed considerably [24,25]. Methane hydrates equally constitute a major potential danger on decomposition affecting the world climate and the sea floor stability of ocean margins [26,27]. Neutrons have played an essential role in elucidating the structure and dynamics of clathrate hydrates. As in ordinary water ice, clathrate hydrates are proton disordered implying structural distortions and thus influencing both the cage stability and guest dynamics. Another interesting manifestation is silicon or germanium-based clathrates [28]. Depending on the nature of the cage as well as on the guest particle the electronic behaviour of these clathrates may range from that of an insulator to a semiconductor or metal.

Textbooks often treat the crystalline world in a very simplified manner. This holds in particular for the vibrational properties that at low frequencies are assumed to be fully accountable for by sound waves. The picture breaks down as soon as a structure contains loosely bound subunits that may vibrate in a much localized fashion at very low frequencies. The transport properties of such systems are often more reminiscent of an amorphous system than of a classical crystalline solid. Clathrates e.g. show heat transport properties, which are very close to those of a glass [29–31]. As heat transport is linked to the scattering of phonons this explains the excitement devoted to the investigation of the lattice dynamics of these systems.

There is, however, an even more fundamental interest. Clathrates constitute a model system which allows one to study the dynamics of particles confined to well-defined cages the size of a few  $\text{\AA}$ . If the cages are assumed to be completely rigid, then the dynamic problem boils down to that of a particle in a potential well. The scientific interest of such a situation is the presence of strong anharmonicities, e.g. in the case of a trough-like well. The elasticity of the cages introduces additional degrees of freedom that allow for the coupling of guest and host vibrations. In simple terms the moving guest deforms the cage when bouncing into it. In clathrates this coupling is essential in the sense

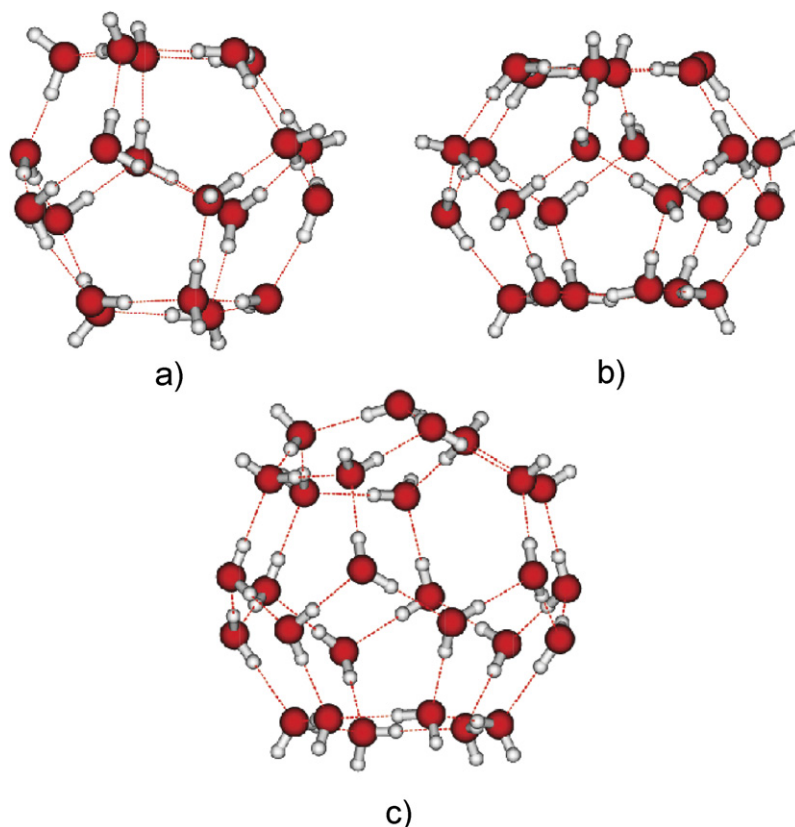


Fig. 7. The three different types of cages in clathrate hydrates: (a) pentagondodecahedron with 12 pentagons ( $5^{12}$ ); (b) tetrakaidecahedron with additional 2 hexagons ( $5^{12}6^2$ ); (c) hexakaidecahedron with additional 4 tetrahedrally arranged hexagons ( $5^{12}6^4$ ). Structure type I clathrate hydrates are formed by cages (a) and (b) in a ratio of 1:3 of small and large cages. Structure type II hydrates are formed by cages (a) and (c) in a ratio 2:1 of small and large cages. The molecular configurations shown respect the ice rules and represent one out of a very large number of possible proton arrangements.

that it prevents the cage from collapsing and thus preserves clathrate stability. The understanding of the dynamics thus becomes a prerequisite for the understanding of stability and formation.

When discussing the dynamics of a guest–host system it is essential to clearly separate the effects of anharmonicity and guest–host coupling. A given system may well show strongly anharmonic behaviour and little coupling and vice versa. A very useful theoretical instrument in this context is the susceptibility  $\chi''(\omega)/\omega$ , which for a single harmonic oscillator is temperature independent and directly related to the inelastic neutron spectra [32] apart from Debye–Waller and multi-phonon corrections. Both corrections cancel each other to a large extent, leading to a basically  $T$ -independence  $\chi''(\omega)/\omega$  for harmonic systems. As proven by Fig. 8 there is little sign of anharmonicity in the guest vibrations of Xe-hydrate at temperatures below some 180 K. The contrary holds for the vibrations of the  $N_2$ -molecules in the small clathrate cages.  $\chi''(\omega)/\omega$  for  $N_2$ -D<sub>2</sub>O as shown in Fig. 9 possesses a well-defined peak that moves to lower frequencies with lower temperatures. It can be well described by a damped harmonic oscillator function (DHO):

$$\omega^{-1}\chi''(\omega) = A \left( \frac{4\omega\Gamma\Omega}{(\omega^2 - \Omega^2)^2 - 4\omega^2\Gamma^2} \right)$$

While the width  $\Gamma$  is constant the squared DHO frequency  $\Omega^2$  scales linearly with temperature. This behaviour is known from classical soft-modes and can be explained by the fact that, as we lower the temperature, the molecules explore the flat part of the cage potential. Extrapolation to zero Kelvin leads to a finite frequency indicating that the molecules finally do get stuck in a multi-well potential. The good description of the  $N_2$  mode softening by a mean field derived DHO indicates that we are dealing with a strongly anharmonic but weakly coupling system.

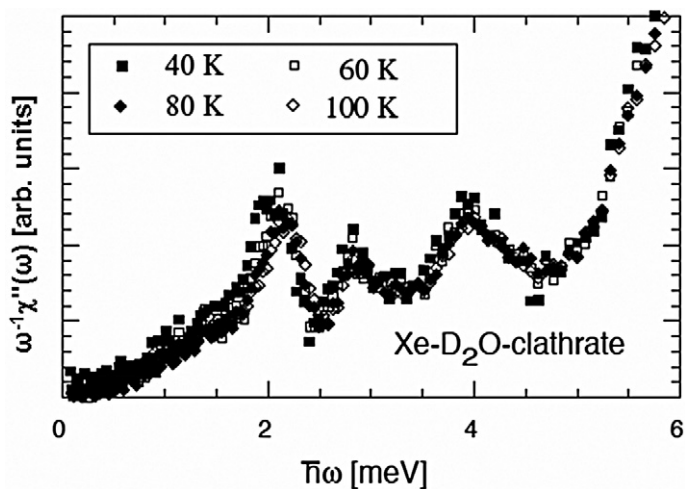


Fig. 8. Dynamic susceptibility multiplied by the inverse frequency as a function of temperature for Xe–D<sub>2</sub>O clathrate. The data have been summed over the scattering angle to achieve better statistics.

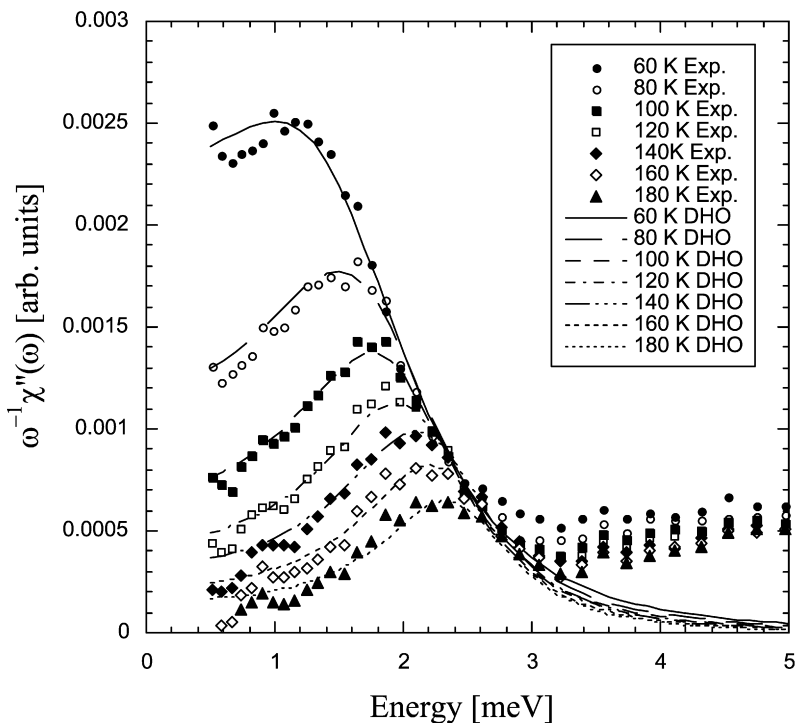


Fig. 9. Dynamic susceptibility multiplied by the inverse frequency as a function of temperature for N<sub>2</sub>–D<sub>2</sub>O clathrate. The data have been summed over the scattering angle to achieve better statistics.

This conclusion is confirmed by the analysis of the N<sub>2</sub>–H<sub>2</sub>O hydrate spectra, which gives no indication of a marked deviation from Debye behavior at low frequencies. The N<sub>2</sub> motions thus do not strongly perturb the acoustic dispersion branches. The opposite behaviour is observed for Xe-hydrate. As already shown by Tse et al. [33,34] the harmonic Xe-modes resonate strongly with the cage and, therefore, become visible in the INS spectra of the protonated samples. The resonance effect can equally be observed in the deuterated Xe–D<sub>2</sub>O hydrate, where it leads to depletion in the Debye region between the Xe-peaks (Fig. 9). Coupling of varying strength has equally been observed in methane hydrate as discussed in detail in [35].

## 5. Conclusion

We have shown that the investigation of the dynamics is indispensable for a good understanding of guest–host systems. Due to the generally weak interaction with the matrix the guest molecules relax easily with the relaxation times falling nicely into the time window of inelastic neutron scattering. In the case of extended cage structures this leads to technologically important diffusion processes. Tailoring the matrix of the host system allows controlling this diffusion process. In a confined space the molecular reorientation opens pathways for chemical processes like polymerization of  $C_{60}$  in carbon nanotubes. In clathrates the internal pressure exerted by the guest on the matrix plays an important role for stability and formation. In all cases inelastic neutron scattering turns out an ideal tool to gain insight into the space and time characteristics of the molecular motion.

## Appendix A

In this part, we give more details about the relation between the scattering cross section  $\frac{\partial^2 \sigma}{\partial \Omega \partial \omega}$ —that is directly measured on a spectrometer—and the other functions that we discuss in this paper i.e. the scattering function  $S(Q, \omega)$ , the generalized density of states (GDOS)  $G(\omega)$  and the ‘susceptibility’  $\chi''(\omega)/\omega$ . Before going further, we would like to precise that these functions are used as convenient representations of the dynamics of the system. In particular, it is necessary to precise here that the GDOS can be compared to the phonon density of states (PDOS) predicted by a calculation keeping in mind that many other corrections might have to be incorporated into the data treatment to precisely match the simulated PDOS. Therefore, many GDOS expressions can be found in the literature each of them being more or less related to the PDOS. Most of the time, it is the nature of the system under study as well as the coherent/incoherent nature of the scattering that will drive the expression of the GDOS. In the following, we are dealing with a powder sample made of pure coherent scatterers. One has to keep in mind that the real PDOS can only be extracted from the measurement of the dispersion curves of the sample which requires large single crystal. Using powder sample, the GDOS is equal to the PDOS only for cubic Bravais lattices at low temperatures.

The powder averaged scattering function  $S(\theta, \omega)$  is easily extracted from the scattering cross section  $\frac{\partial^2 \sigma}{\partial \Omega \partial \omega}$  using the expression  $\frac{\partial^2 \sigma}{\partial \Omega \partial \omega} = \frac{k_d}{k_i} S(\theta, \omega)$  with  $\Omega$  the scattering solid angle and  $\vec{k}_i$  and  $\vec{k}_d$  the incident and scattered neutron wave vectors respectively.  $\theta$  is the scattering angle and stands as the angle between  $\vec{k}_i$  and  $\vec{k}_d$ . An interpolation scheme can be used to further transform the scattering function expressed in the  $(\theta, \omega)$  coordinate,  $S(\theta, \omega)$ , into the more physically meaningful scattering function expressed in the  $(Q, \omega)$  coordinate system,  $S(Q, \omega)$ . The intermediate scattering function  $I(Q, t)$  is related to the scattering function  $S(Q, \omega)$  by an inverse time Fourier transformation:  $I(Q, t) = \int_{-\infty}^{\infty} S(Q, \omega) \exp(i\omega t) d\omega$ . The intermediate scattering function can directly be measured using spin-echo spectrometer.

The Generalized Density Of States  $G(\hat{\theta}, \omega)$  that is used in Section 3 can be written as follows:  $G(\hat{\theta}, \omega) = \frac{S(\hat{\theta}, \omega)}{Q^2(\hat{\theta}, \omega)} \times B(\omega, T)$  where  $\hat{\theta}$  refers to the averaged scattering angle, and  $S(\hat{\theta}, \omega) = \frac{1}{N_D} \sum_i S(\theta_i, \omega)$  with  $i$  ranging from the first to the last detector considered in the summation and  $\theta_i$  is the angle corresponding to this detector.  $N_D$  is the total number of detectors, and  $Q^2(\hat{\theta}, \omega)$  is the scattering vector which is calculated at each energy transfer for the averaged scattering angle.  $B(\omega, T)$  is a function accounting for the population of the modes with temperature  $T$ :  $B(\omega, T) = \hbar\omega(1 - \exp(-\frac{\hbar\omega}{kT}))$ . Note that  $\hbar\omega$  is negative when the energy transfer is from the sample to the neutron (anti-Stokes or down scattering or neutron energy gain) i.e.  $\hbar\omega = E_i - E_d$  and  $E_i$  and  $E_d$  refer to the incident and scattered energy of the neutron respectively. A more detailed discussion of the derivation of a density-of-states from neutron data can be found in [36].

The ‘susceptibility’  $\chi''(\omega)/\omega$  is expressed simply as  $\frac{\chi''(\omega)}{\omega} = \frac{1}{N_D} \sum_i S(\theta_i, \omega) \times \frac{B(\omega, T)}{|\hbar\omega|}$ .

An important precision is that the GDOS and the susceptibility are obtained after an averaging over the scattering angles considered in the experiment. Such an averaging is performed to improve the statistics and to smooth out the coherence effects of the scattering. This is the so-called incoherent approximation. As a result, the susceptibility and the GDOS might be slightly spectrometer dependent with regards to the scattering angle and wavelength available.

## References

- [1] J. Kärger, D.M. Ruthven, Diffusion in Zeolites and Other Microporous Solids, Wiley, New York, 1992.

- [2] H. Jobic, J. Kärger, M. Bée, *Phys. Rev. Lett.* 82 (1999) 4260.
- [3] J.P. Hoogenboom, H.L. Tepper, N.F.A. van der Vegt, W.J. Briels, *J. Chem. Phys.* 113 (2000) 6875.
- [4] E.J. Maginn, A.T. Bell, D.N. Theodorou, *J. Phys. Chem.* 100 (1996) 7155.
- [5] H. Jobic, *J. Mol. Catal. A* 158 (2000) 135.
- [6] H. Jobic, W. Schmidt, C.B. Krause, J. Kärger, *Micropor. Mesopor. Mater.* 90 (2006) 299.
- [7] H. Jobic, D.N. Theodorou, *J. Phys. Chem.* 110 (2006) 1964.
- [8] H. Jobic, A. Méthivier, G. Ehlers, B. Farago, W. Haeussler, *Angew. Chem. Int. Ed.* 43 (2004) 364.
- [9] R.L. Goring, *J. Catal.* 31 (1973) 13.
- [10] A. Loiseau, P. Launois, P. Petit, S. Roche, J.-P. Salvetat (Eds.), *Understanding Carbon Nanotubes*, Lect. Notes in Phys., vol. 667, Springer, Berlin/Heidelberg, 2007.
- [11] S. Rols, Z. Benes, E. Anglaret, J.-L. Sauvajol, P. Papanek, J.E. Fischer, G. Coddens, H. Schober, A.J. Dianoux, *Phys. Rev. Lett.* 85 (2000) 5222.
- [12] A.I. Kolesnikov, J.-M. Zanotti, C.-K. Loong, P. Thiyagarajan, A.P. Moravsky, R.O. Loutfy, *Phys. Rev. Lett.* 93 (2004) 035503.
- [13] R. Pfeiffer, H. Kuzmany, T. Pichler, H. Kataura, Y. Achiba, M. Melle-Franco, F. Zerbetto, *Phys. Rev. B* 69 (2004) 035404.
- [14] J.R.D. Copley, D.A. Neumann, R.L. Cappelletti, W.A. Kamitakahara, *J. Phys. Chem. Solids* 53 (1992) 1353.
- [15] L. Pintschovius, *Rep. Prog. Phys.* 59 (1996) 473.
- [16] P.A. Heiney, *J. Phys. Chem. Solids* 53 (1992) 1333.
- [17] B. Renker, F. Gompf, H. Schober, P. Adelman, H.J. Bornemann, R. Heid, *Z. Phys. B* 92 (1993) 451.
- [18] S. Rols, J. Cambedouzou, J.-L. Bantignies, F. Rachdi, J.-L. Sauvajol, V. Agafonov, A.V. Rakhmanina, V.A. Davydov, B. Hennion, R. Kahn, *Phys. Rev. B* 70 (2004) 104302.
- [19] J. Cambedouzou, S. Rols, R. Almairac, J.-L. Sauvajol, H. Kataura, H. Schober, *Phys. Rev. B* 71 (2005) R041403.
- [20] M. Chorro, S. Rols, J. Cambedouzou, L. Alvarez, R. Almairac, J.-L. Sauvajol, J.-L. Hodeau, L. Marques, M. Mezouar, H. Kataura, *Phys. Rev. B* 74 (2006) 205425.
- [21] S. Rols, R. Almairac, E. Bretszajn, V.A. Agafonov, A.V. Rakhmanina, V.A. Davydov, in preparation.
- [22] G. Dresselhaus, M.S. Dresselhaus, P.C. Ecklund, *Phys. Rev. B* 45 (1992) 6923.
- [23] J. Cambedouzou, Ph.D. Thesis, University of Montpellier, 2004.
- [24] E.D. Sloan Jr., *Clathrate Hydrate of Natural Gases*, second ed., Dekker, New York, 1998.
- [25] M.D. Max, *Natural Gas Hydrate in Oceanic and Permafrost Environments*, Kluwer, Dordrecht, 2000.
- [26] J.P. Henriot, J. Mienert, *Gas Hydrates—Relevance to World Margin Stability and Climatic Change*, Geolog. Soc., London, 1998.
- [27] W.T. Wood, J.F. Gettrust, N.R. Chapman, G.D. Spencer, R.D. Hynman, *Nature* 420 (2002) 656.
- [28] J.S. Kasper, P. Hagenmüller, M. Pouchard, C. Cros, *Science* 150 (1965) 1713.
- [29] P. Andersson, R.G. Ross, *J. Phys. C: Solid State Phys.* 16 (1983) 1423.
- [30] J.S. Tse, M.A. White, *J. Phys. Chem.* 92 (1988) 5006.
- [31] J.L. Cohn, G.S. Nolas, V. Fessatidis, T.H. Metcalf, G.A. Slack, *Phys. Rev. Lett.* 82 (1999) 779.
- [32] H. Schober, A. Tölle, B. Renker, R. Heid, F. Gompf, *Phys. Rev. B* 56 (1997) 5937.
- [33] J.S. Tse, V.P. Shpakov, V.R. Belosludov, F. Trouw, Y.P. Handa, W. Press, *Europhys. Lett.* 54 (2001) 354.
- [34] C. Gutt, J. Baumert, W. Press, J.S. Tse, S. Janssen, *J. Chem. Phys.* 116 (2002) 3795.
- [35] J. Baumert, C. Gutt, V.P. Shpakov, J.S. Tse, M. Krisch, M. Müller, H. Requardt, D.D. Klug, S. Janssen, W. Press, *Phys. Rev. B* 68 (2003) 174301.
- [36] H. Schober, *J. Phys. IV* 103 (2003) 173.